



## Analyzing Remote Sensing Data in R: The landsat Package

Sarah C. Goslee

USDA-ARS Pasture Systems and Watershed Management Research Unit

---

### Abstract

Research and development on atmospheric and topographic correction methods for multispectral satellite data such as Landsat images has far outpaced the availability of those methods in geographic information systems software. As Landsat and other data become more widely available, demand for these improved correction methods will increase. Open source R statistical software can help bridge the gap between research and implementation. Sophisticated spatial data routines are already available, and the ease of program development in R makes it straightforward to implement new correction algorithms and to assess the results. Collecting radiometric, atmospheric, and topographic correction routines into the **landsat** package will make them readily available for evaluation for particular applications.

*Keywords:* atmospheric correction, Landsat, radiometric correction, R, remote sensing, satellite, topographic correction.

---

## 1. Introduction

Satellite remote sensing data can provide a complement or even alternative to ground-based research for large scale studies or over long periods. The Landsat platform is the premier example: images have been collected continuously since the early 1970s. If both Landsat 5 and 7 are considered, every location within the United States is imaged every 8 days. Other satellite platforms have become available more recently. Images from all platforms can be used for mapping land cover, tracking land use change, and even estimating plant biomass.

Image characteristics vary from date to date. Some of this variation is due to solar elevation angle and can be easily corrected for given date and time (radiometric calibration). Additional variation is caused by atmospheric conditions at the time of imaging: scatter at different wavelengths due to haze. Atmospheric corrections are very complex. If one image every few

years is analyzed, for example to track development patterns, atmospheric corrections may be unnecessary because of the magnitude of the change in land use during that interval. If researchers wish to take advantage of the temporal data density offered by Landsat, careful correction is required. Otherwise differences in apparent reflectance due to atmospheric variation can swamp differences caused by actual change on the ground. In mountainous areas, topographic corrections are also necessary to compensate for differences in incident radiation due to slope and aspect. Without correction, the same ground cover on opposite sides of the mountain could return a different signal.

Many procedures to implement atmospheric and topographic corrections have been proposed, each with strengths and weaknesses, but few are readily available in geographic information systems (GIS) or image processing software. It is impossible to compare methods to identify the one most suited for a given application. Indeed, it is not always clear exactly what proprietary GIS software is doing. R offers an alternative to GIS software for research and testing of satellite image processing algorithms. The interpreted nature of R makes it possible to implement, test and modify algorithms easily. The available graphical and statistical tools are vastly superior to anything available in common GIS packages, making it straightforward to compare algorithms. Tools for processing and display of spatially-referenced data are already available in R (R Development Core Team 2011). The **sp** (Bivand, Pebesma, and Gomez-Rubio 2008) and **rgdal** (Keitt, Bivand, Pebesma, and Rowlingson 2011) packages provide these capabilities for several commonly-used spatial formats.

The **landsat** package described here, and available from the Comprehensive R Archive Network at <http://CRAN.R-project.org/package=landsat>, provides basic tools for working with satellite imagery such as automated georeferencing and cloud detection. It contains functions for radiometric normalization, and several different approaches to atmospheric correction. Four topographic correction algorithms have been implemented. Other useful functions such as bare soil line and tasseled cap calculations have been included. While these functions were developed with Landsat data in mind, they are suitable for use with satellite imagery from other platforms as long as appropriate calibration data are used.

## 2. Landsat platform characteristics

Landsat 5 (TM) was launched on 1984-03-01 and Landsat 7 (ETM+) on 1999-04-15. Each revisits a location every 16 days, and the two orbits are staggered so an image is taken for each location every 8 days. The Landsat Data Continuity Mission is planned to launch in 2011, and will record data in bands compatible with the TM and ETM+ instruments. Due to a hardware failure on 2003-05-31, Landsat 7 scenes are now missing 22% of the pixels. The problem is most severe near the edges of a image. Band characteristics are largely consistent, but ETM+ added an additional band (Table 1).

The Landsat images have been converted to integer digital numbers (*DN*) before distribution to facilitate storage and display. They may require conversion to radiance or reflectance, topographic correction or atmospheric correction. If using a single image, or images widely separated in time to examine gross changes, minimal processing may be required. For detailed comparison of vegetation indices from multiple images, however, careful correction is needed. The most accurate atmospheric corrections require ground data taken during the satellite overpass. For retrospective studies this is impossible to obtain, and less-accurate image-based

		Landsat 5		
		Planned wavelength	Actual wavelength	Resolution
Band 1	Blue	0.45–0.52	0.452–0.518	30
Band 2	Green	0.52–0.60	0.528–0.609	30
Band 3	Red	0.63–0.69	0.626–0.693	30
Band 4	Near infrared (NIR)	0.76–0.90	0.776–0.904	30
Band 5	Middle infrared (MIR)	1.55–1.75	1.567–1.784	30
Band 6	Thermal infrared (TIR)	10.40–12.50	10.45–12.42	120
Band 7	Middle infrared (SWIR)	2.08–2.35	2.097–2.349	30
		Landsat 7		
		Planned wavelength	Actual wavelength	Resolution
Band 1	Blue	0.45–0.52	0.452–0.514	30
Band 2	Green	0.52–0.60	0.519–0.601	30
Band 3	Red	0.63–0.69	0.631–0.692	30
Band 4	Near infrared (NIR)	0.77–0.90	0.772–0.898	30
Band 5	Middle infrared (MIR)	1.55–1.75	1.547–1.748	30
Band 6	Thermal infrared (TIR)	10.40–12.50	10.31–12.36	60
Band 7	Middle infrared (SWIR)	2.09–2.35	2.065–2.346	30
Band 8	Panchromatic	0.52–0.90	0.515–0.896	15

Table 1: Band wavelengths ( $\mu m$ ) and resolutions ( $m$ ) for Landsat 5 Thematic Mapper (TM) and 7 Enhanced Thematic Mapper (ETM+). Band 8 (ETM+ only) is higher-resolution visible light data. Actual wavelengths are from [Chander \*et al.\* \(2009\)](#).

correction methods must be used. The following sections describe the procedures needed for calibration of Landsat data and the R implementations of these algorithms in the **landsat** package.

### 3. Sample data

The **landsat** package includes a  $300 \times 300$  pixel subset of United States Geological Survey (USGS) Landsat ETM+ images from two dates, 2002-07-20 and 2002-11-25 ([US Geological Survey 2010b](#)). These images are in `SpatialGridDataFrame` format, and can be displayed using `image()`. Even after clouds are removed, the July image has a higher mean  $DN$  and greater dynamic range than the November image (Figure 1c, d). Complete metadata are included in the help files. A USGS digital elevation model (DEM) covering the same area and at the same resolution has been included (Figure 1f; [US Geological Survey 2010a](#)).

### 4. Tools

This package provides a few basic tools for working with Landsat images. The `lssub()` function is an R interface to the image subsetting tools from the Geospatial Data Abstraction Library (GDAL, [GDAL Development Team 2011](#)). This function is provided for convenience; while the same effect can be obtained using the subsetting property of `sp`, it is considerably faster to use the GDAL functions to remove a smaller section of a geotiff image. Landsat images are usually distributed as geotiff files, and can be imported in `SpatialGridDataFrame`

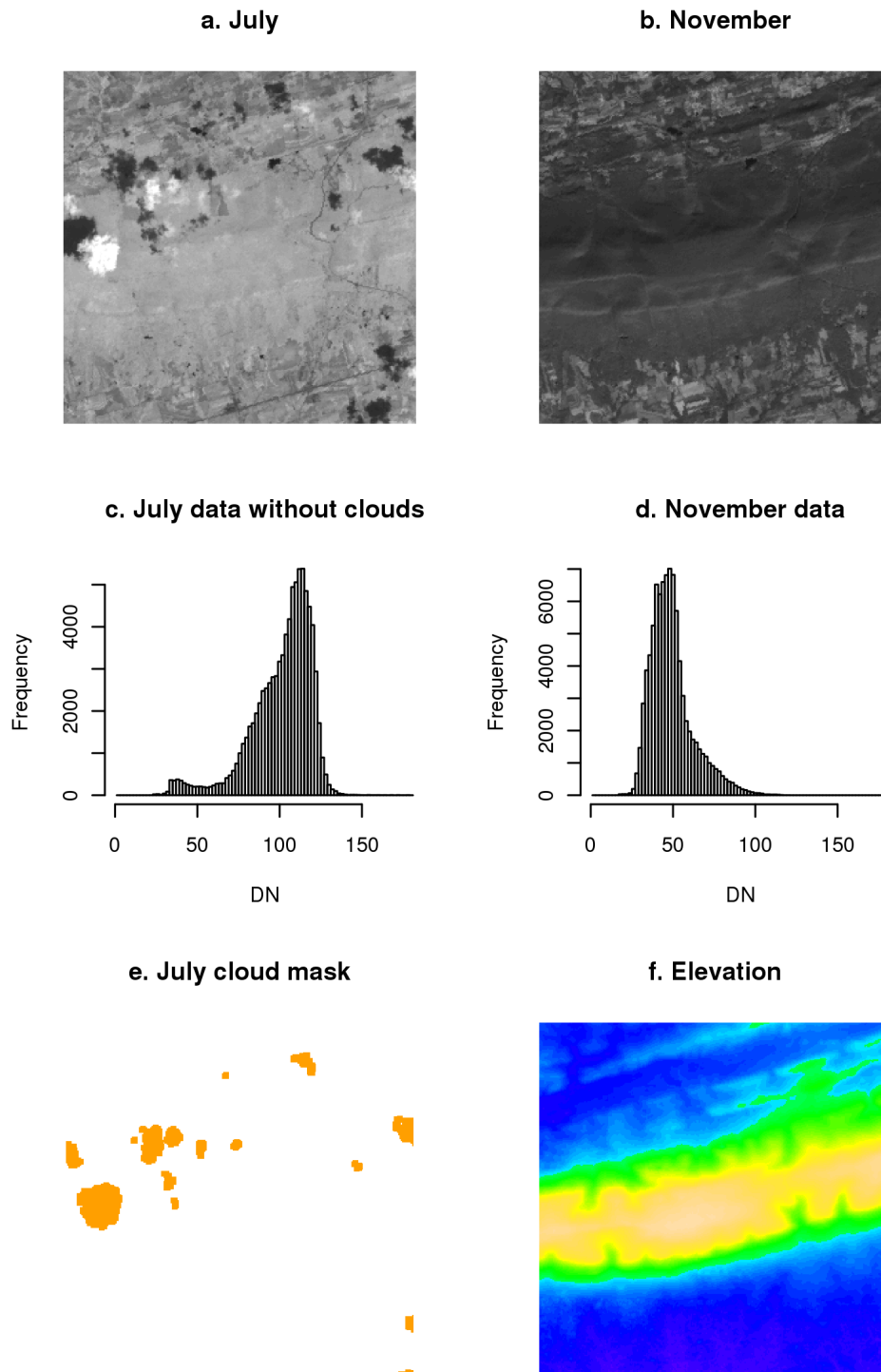


Figure 1: Band 4 (near infrared) from Landsat images from July and November 2002. The July image has substantial cloud cover, as identified in the cloud mask produced by `clouds()`. November 2002 was cloud-free, so no mask is shown.

format using `readGDAL`. The `lssub()` function preserves the geotiff format.

Image processing requires some information not often available in the metadata. The Earth-Sun distance for a given date can be calculated with `ESdist()`. A date can be conveniently converted to decimal format with `ddist()`.

#### 4.1. Automated georeferencing

A simple error-minimization routine can be used to provide relative georeferencing by matching one image to a reference image (`georef` and `geoshift` by means of vertical and horizontal shifts. If the reference image has been absolutely georeferenced, then all of the subsequent images will also be spatially referenced. This function can find local minima, so results should always be checked visually. The matching process only needs to be done once for each date; Band 3 or Band 4 generally provide good results, but any band may be used. The results of this step can then be used for each band image from that date. Sufficient padding must be added around the edges of the image to accommodate the magnitude of the shift. The larger the image area, the more effective the matching process. The below example illustrates the procedure, but because of the small image sizes used for the demo data the shift coefficients are unreliable.

```
R> july.shift <- georef(nov3, july3, maxdist = 50)
R> july1.corr <- geoshift(july1, padx = 10, pady = 10, july.shift$shiftx,
+   july.shift$shifty)
```

#### 4.2. Topographic calculations

Topographic corrections require the use of slope and aspect data calculated from a DEM of the same resolution as the satellite data. The `slopeasp()` function will calculate both given a DEM. While all GIS software will provide topographic calculations, this function was included for the convenience of being able to do all the processing within R and to allow exploration of different algorithms. Most GIS software offers only a tiny subset of the methods that have been proposed.

The most common method for slope and aspect calculations is the third-order finite difference weighted by reciprocal of distance (Unwin 1981; Clarke and Lee 2007). This method is the equivalent of using a  $3 \times 3$  Sobel filter to determine the east-west slope and the north-south slope. Given a cell  $Z_{i,j}$  with east-west cell size  $EW_{res}$  and north-south cell size  $NS_{res}$ , slope in either percent or degrees, and aspect with north as  $0^\circ$ , east as  $90^\circ$  and south as  $180^\circ$  can be calculated using Equation 1. A simple smoothing correction (dividing by a smoothing parameter before taking the arctan) can reduce extreme slope values (Riano, Chuvieco, Salas, and Aguado 2003).

$$\begin{aligned}
 EW &= [(Z_{i+1,j+1} + 2Z_{i+1,j} + Z_{i+1,j-1}) - (Z_{i-1,j+1} + 2Z_{i-1,j} + Z_{i-1,j-1})]/(8EW_{res}) \\
 NS &= [(Z_{i+1,j+1} + 2Z_{i,j+1} + Z_{i-1,j+1}) - (Z_{i+1,j-1} + 2Z_{i,j-1} + Z_{i-1,j-1})]/(8NS_{res}) \\
 \theta_p &= \arctan \sqrt{EW^2 + NS^2} \\
 slope\% &= 100 \cdot \sqrt{EW^2 + NS^2} \\
 \phi_o &= 180^\circ - \arctan \left( \frac{NS}{EW} \right) + 90^\circ \frac{EW}{|EW|}
 \end{aligned} \tag{1}$$

## 5. Radiometric calibration

Landsat images are distributed as digital numbers, integer values from 0–255. While less crucial now, this correction was originally necessary to make it possible to store, distribute and portray these images efficiently. Radiometric calibration is a two-step process. First the  $DN$  values are converted to at-satellite radiance using parameters provided in the image metadata. Data on solar intensity are used to convert the at-satellite radiance to at-satellite reflectance. These parameters are also in the image metadata.

### 5.1. At-sensor radiance

The first step in processing is to convert  $DN$  to at-sensor spectral radiance  $L$ , also called top-of-atmosphere radiance. The conversion coefficients are available in the metadata accompanying the images. Whenever possible the metadata values should be used, as coefficients vary by platform and over time, but standard coefficients are given in Table 2.

Coefficients are provided in one of three band-specific formats:  $gain_2$  and  $offset$ ;  $G_{rescale}$  (also called gain) and  $B_{rescale}$  (bias); or radiances associated with minimum and maximum  $DN$  values ( $L_{max}$  and  $L_{min}$ ). Any of the three can be used to convert from  $DN$  to at-sensor radiance (Equation 2).

$$L = \frac{DN - offset}{gain_2}$$

$$L = G_{rescale}DN + B_{rescale} \tag{2}$$

$$L = \left( \frac{L_{max} - L_{min}}{DN_{max} - DN_{min}} \right) \cdot (DN - DN_{min}) + L_{min}$$

It is not always clear which form of coefficients the metadata contain because “gain” has been used to refer to both  $gain_2$  and  $G_{rescale}$ . Most recent image metadata provide  $G_{rescale}$  and  $B_{rescale}$ , but these formulations are interconvertible (Equation 3). The magnitudes of  $G_{rescale}$  and  $gain_2$  are similar for most bands, but the former is paired with  $B_{rescale}$ , which will have

	Landsat 5		Landsat 7 low gain		Landsat 7 high gain	
	$G_{rescale}$	$B_{rescale}$	$G_{rescale}$	$B_{rescale}$	$G_{rescale}$	$B_{rescale}$
Band 1	0.765827	-2.29	1.180709	-7.38	0.778740	-6.98
	0.671339	-2.19	<i>for TM images taken before 1991-12-31</i>			
Band 2	1.448189	-4.29	1.209843	-7.61	0.798819	-7.20
	1.322205	-4.16	<i>for TM images taken before 1991-12-31</i>			
Band 3	1.043976	-2.21	0.942520	-5.94	0.621654	-5.62
Band 4	0.876024	-2.39	0.969291	-6.07	0.639764	-5.74
Band 5	0.120354	-0.49	0.191220	-1.19	0.126220	-1.13
Band 6	0.055376	1.18	0.067087	-0.07	0.037205	3.16
Band 7	0.065551	-0.22	0.066496	-0.42	0.043898	-0.39
Band 8	NA	NA	0.975597	-5.68	0.641732	-5.34

Table 2: Default gain ( $G_{rescale}$ ;  $Wm^{-2}sr^{-1}\mu m^{-1}DN^{-1}$ ) and bias ( $B_{rescale}$ ;  $Wm^{-2}sr^{-1}\mu m^{-1}$ ) for Landsat 5 (TM) and Landsat 7 (ETM) from [Chander et al. \(2009\)](#). The metadata will state whether Landsat 7 images were taken at low gain or high gain.

	Landsat 5	Landsat 7
Band 1	1983	1997
Band 2	1796	1812
Band 3	1536	1533
Band 4	1031	1039
Band 5	220.0	230.8
Band 7	83.44	84.90
Band 8	NA	1362

Table 3: Extra-solar atmospheric constants ( $E_{sun}$ ;  $Wm^{-2}\mu m^{-1}$ ) for Landsat 5 (TM) and 7 (ETM+) from Chander *et al.* (2009). (Note: The Landsat 5 column contained errors in previous versions of this manuscript, corrected on 2012-01-08.)

negative values for non-thermal bands, while  $gain_2$  is paired with  $offset$ , which is positive for non-thermal bands.

$$\begin{aligned}
 G_{rescale} &= \frac{L_{max} - L_{min}}{DN_{max} - DN_{min}} \\
 G_{rescale} &= \frac{1}{gain_2} \\
 B_{rescale} &= L_{min} - G_{rescale} DN_{min} \\
 B_{rescale} &= \frac{-offset}{gain_2} \\
 gain_2 &= \frac{1}{G_{rescale}} \\
 offset &= \frac{-B_{rescale}}{G_{rescale}}
 \end{aligned} \tag{3}$$

All radiometric functions in **landsat** accept either  $gain$  and  $offset$  or  $G_{rescale}$  and  $B_{rescale}$ .

## 5.2. At-sensor reflectance

The at-sensor radiance values calculated using Equation 2 must be corrected for solar variability caused by annual changes in the Earth-Sun distance  $d$ , producing unitless at-sensor (or top-of-atmosphere) reflectance  $\rho_{AS}$  (Equation 4).

$$\rho_{AS} = \frac{\pi d^2 L}{E_{sun} \cos \theta_z} \tag{4}$$

$E_{sun}$  is the band-specific exoatmospheric solar constant (Table 3;  $Wm^{-2}\mu m^{-1}$ ). The solar zenith angle  $\theta_z$  can be derived from the image metadata, where the solar elevation angle  $\theta_s$  is usually included;  $\theta_z = 90^\circ - \theta_s$ . At-sensor reflectance can be calculated using the `radiocorr()` function with `method = "apparentreflectance"`.

```
R> july4.ar <- radiocorr(july4, Grescale = 0.63725, Brescale = -5.1,
+   sunelev = 61.4, edist = ESdist("2002-07-20"), Esun = 1039,
+   method = "apparentreflectance")
```

### 5.3. Thermal bands

Band 6 contains thermal infrared data. Landsat 7 offers two thermal bands, while Landsat 5 provides one. Instead of calculating top-of-atmosphere reflectance, these data can be converted to temperature ( $K^\circ$ ) using `thermalband()`. This function provides default coefficients, and requires only the *DN* data and the band number (6 for Landsat 5; 61 or 62 for Landsat 7).

```
R> july61.thermal <- thermalband(july61, band = 61)
```

## 6. Cloud identification

Clouds are reflective (high) in Band 1 and cold (low) in Band 6, so the ratio of the two bands is high over clouds (Martinez, Gould, and González 2007). The absolute value of this ratio must be adjusted for data type, whether reflectance, radiance, or *DN*. The `clouds()` function will create a cloud mask (1 where clouds are present; NA where they are not) given Band 1 and Band 6. The default parameters for the ratio level (`level`) and for adding a buffer around the cloud edge (`buffer`) were adequate for the test data once converted to at-sensor reflectance and temperature. This function can be used with *DN* data if the `level` argument is adjusted appropriately. The mask does not demarcate areas of cloud shadow, but only the clouds themselves (Figure 1e).

```
R> july.cloud <- clouds(july1.ar, july61.thermal)
R> nov.cloud <- clouds(nov1.ar, nov61.thermal)
```

## 7. Atmospheric correction

For most applications, ground reflectance is of greater interest than at-sensor reflectance so atmospheric correction is required. Variation in atmospheric conditions at the time of overpass can overwhelm any changes in surface reflectance, so it is crucial to correct for these differences. If measured atmospheric data such as optical depth are available an accurate correction can be applied, but these are rarely available for retrospective studies. Most commonly, an image-based method is used instead. Two categories of corrections are available. Relative normalization methods match the spectral characteristics of each image to a reference image in such a way that each transformed image appears to have been taken using the same sensor and with the same atmospheric conditions as the reference image. Functions are available for relative atmospheric correction methods using the entire image or unchanging subsets.

Absolute atmospheric correction methods rely on a mechanistic understanding of atmospheric effects to adjust each image individually. Instead of correcting to a reference image, information contained in part of an image, for instance the darkest areas, is extracted and used to correct the rest of the image. This extracted information substitutes for measured parameters. Three such methods have been included here.

### 7.1. Relative atmospheric correction using the entire image

Statistical correction methods are entirely empirical and do not consider physical principles

or atmospheric conditions in any way. These algorithms force the distribution of values in one image to match that in another. Unless otherwise indicated, these methods can operate on *DN* or reflectance.

### *Relative normalization*

The most aggressive correction method is to regress all of the pixels in the image to be corrected onto the corresponding pixels in the reference image. This method requires georeferenced images covering the same area and at the same resolution. Since both variables are random, model II regression method such as Major Axis regression implemented in `lmodel2()` from the **lmodel2** package is recommended (Legendre 2008). The `relnorm()` function implements this method for spatial data, and returns both a corrected image and the coefficients used. In the example given here, Band 4 of the July image is corrected to match the November image.

```
R> july4.rncoef <- relnorm(nov4, july4, mask = july.cloud, nperm = 0)
R> july4.rn <- july4.rncoef[["newimage"]]
```

### *Histogram matching*

Histogram matching forces the distribution of the *DN* values in one image to match another. This algorithm is commonly used in other areas of image processing, and the images do not need to cover the same area, or to match in any way. The `histmatch()` function should be used only with the integer *DN* values. In the example given here, Band 4 of the July image is corrected to match the November image.

```
R> july4.hmcoef <- histmatch(nov4, july4, mask = july.cloud)
R> july4.hm <- july4.hmcoef[["newimage"]]
```

For this image pair, histogram matching performs better than relative normalization (Figure 2). The former method forces the histogram for July to acquire the shape of the histogram for November, while keeping the range of values (compare Figure 1c to Figure 2c). Relative normalization created a similar histogram profile, but greatly compressed the dynamic range, thereby losing much of the information contained in the data. This method also inverted the values of the original image: the slope of the regression line was negative. This inversion is a drawback of relative normalization methods, especially for image pairs where seasonal vegetation differences are pronounced.

## **7.2. Relative atmospheric correction using a subset of the image**

Using the entire image for statistical correction includes areas of the image that are likely to change between dates, particularly vegetation, so the correction factors incorporate non-atmospheric effects. As shown above this may have unwanted side effects. These corrections may thus conceal actual changes between dates. Identifying pixels that cover developed areas or other land uses that would be expected to possess constant reflectance properties from date to date could produce more accurate statistical corrections. Two methods for doing so are included in **landsat**: pseudo-invariant features and radiometric control sets.

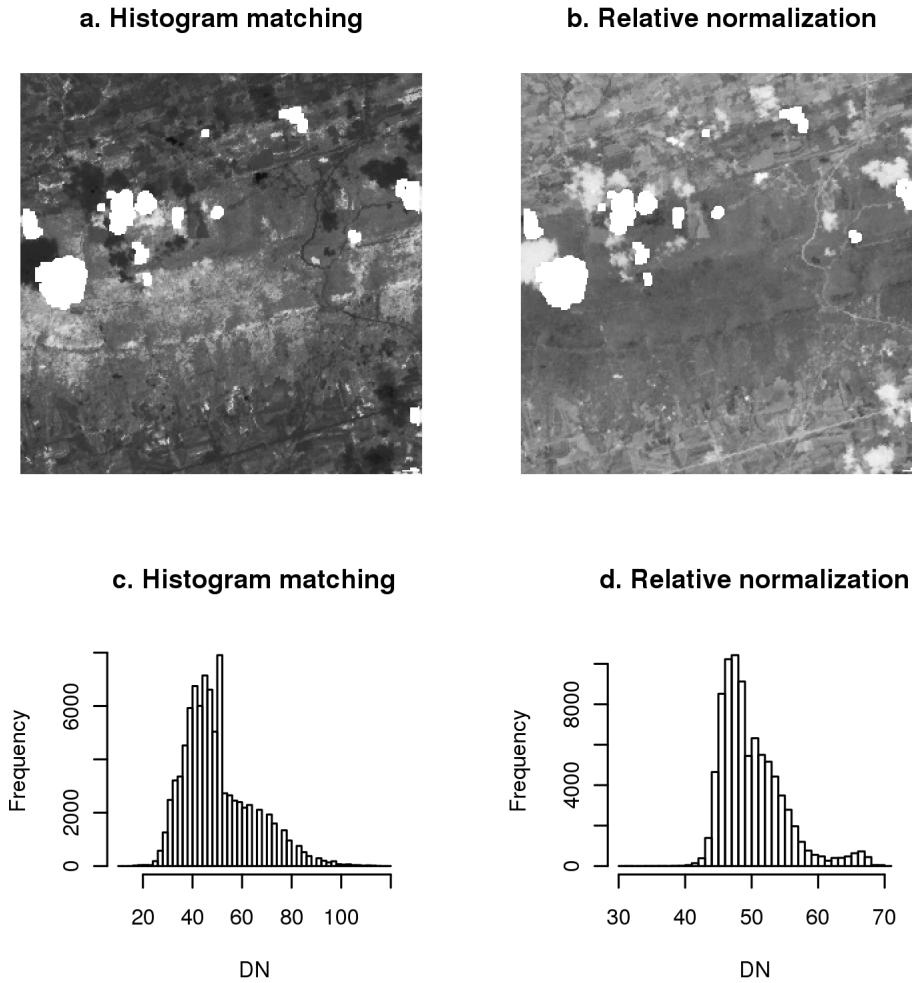


Figure 2: Whole-image relative atmospheric corrections for Band 4 of the July data.

### *Pseudo-invariant features*

The reflectance of a specific developed area such as a large rooftop or parking lot should not change seasonally, so differences in apparent reflectance in these areas between dates are assumed to be due to atmospheric differences. Such areas, termed pseudo-invariant features (PIF) by [Schott, Salvaggio, and Volchok \(1988\)](#), can be identified using Band 7 and the ratio of Band 4 to Band 3. The Band 4 to Band 3 ratio is low where there is no vegetation, including water and developed areas. Band 7 is low over water areas, so it can be used to distinguish between the unvegetated areas identified using the Band 4 to Band 3 ratio. As implemented here, the images must cover the same area at the same resolution, but that is not a requirement of the method. The `PIF()` function can be used to identify invariant features within an image using the above criteria. Visual inspection may be needed to ensure that the threshold value is correct for the particular images being analyzed. Having an insufficient number of PIF points is a concern with this method, especially with the small images in these examples.

Using the data included in the **landsat** package, November is the clearer image, as would be expected because of the higher humidity in the summer months, so it is used to identify PIF pixels. These PIFs are then used in major axis regression to correct the July image (only Band 4 is shown).

```
R> nov.PIF <- PIF(nov3, nov4, nov7, level = 0.9)
R> july4.pifcorr <- lmodel2(nov4@data[nov.PIF@data[, 1] == 1, 1] ~
+   july4@data[nov.PIF@data[, 1] == 1, 1])
R> july4.pifcorr <- unlist(july4.pifcorr[["regression.results"]][2, 2:3])
```

The final steps in the correction are to use the original image as a template for putting the corrected data into the **SpatialGridDataFrame** format, and to block out the previously-identified cloud areas.

```
R> july4.pif <- july4
R> july4.pif@data[, 1] <- july4@data[, 1] * july4.pifcorr[2] +
+   july4.pifcorr[1]
R> july4.pif@data[!is.na(july4.cloud@data[, 1]), 1] <- NA
```

### *Radiometric control sets*

The radiometric control set (RCS) procedure implemented in **RCS()** takes a different approach to choosing invariant features [Hall, Strebel, Nickeson, and Goetz \(1991\)](#). The tasseled cap procedure (**tasscap()**) is used to identify the greenness and brightness components of the image ([Crist 1985](#); [Crist and Kauth 1986](#); [Huang, Wylie, Yang, Homer, and Zylstra 2002](#)). These are then used to identify dark sets and bright sets with low greenness: unvegetated radiometric control sets. As with **PIF()**, the threshold value may need to be adjusted for a particular set of images. The tasseled-cap procedure included in **landsat** contains default values for at-sensor reflectance for both Landsat 5 (TM) and 7 (ETM+), although other formulations are available in the literature. In the example given, reflectance is used for RCS identification, but the adjustment is done on the *DN* values to maintain consistency with previous correction examples.

The clearer November image is used to identify the radiometric control set, and major axis regression is used to correct the July image based on that RCS. Finally the corrected data are put in **SpatialGridDataFrame** format, and cloud areas removed.

```
R> nov.tasscap <- tasscap("nov", 7)
R> nov.RCS <- RCS(nov.tasscap)
R> july4.rcscorr <- lmodel2(nov4@data[nov.RCS@data[, 1] == 1, 1] ~
+   july4@data[nov.RCS@data[, 1] == 1, 1])
R> july4.rcscorr <- unlist(july4.rcscorr[["regression.results"]][2, 2:3])
R> july4.rcs <- july4
R> july4.rcs@data[, 1] <- july4@data[, 1] * july4.rcscorr[2] +
+   july4.rcscorr[1]
R> july4.rcs@data[!is.na(july4.cloud@data[, 1]), 1] <- NA
```

The PIF correction compressed the range of *DN* values considerably (Figure 3c), losing much of the detail in the original image (Figure 1a). Using only points identified by **PIF()** for both

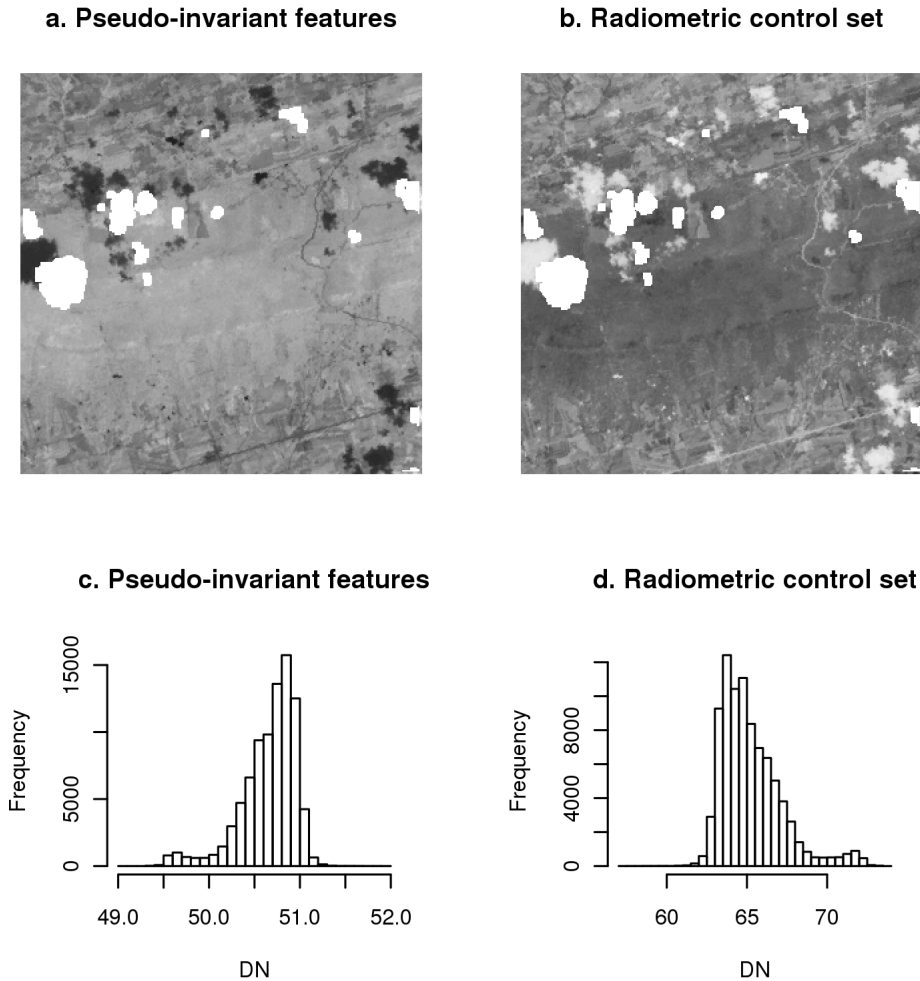


Figure 3: Subset-based relative atmospheric corrections for Band 4 of the July data.

dates, rather than just in the clearer November image set, did not improve the results. The RCS correction reduced the dynamic range somewhat, and inverted the data range, as did relative normalization (Figure 3d; Figure 2d). Of the four whole-image relative atmospheric correction methods implemented here, only the histogram matching method produced acceptable results.

The root mean square error ( $RMSE$ ) between the target and reference image can be used to assess the effectiveness of a relative correction. The greater the reduction in  $RMSE$ , the more effective the transformation was at matching that image pair. The  $RMSE$  for the untransformed Band 4 data was 0.2, and after histogram matching it was reduced to 0.067. Despite their poor overall performance in other ways, the other three methods reduced  $RMSE$  values as much or more: 0.043 for relative normalization, 0.043 for PIF, and 0.065 for RCS. The correspondence between image pairs can increase even when other properties such as range that are crucial for further analysis and interpretation are not preserved.

### 7.3. Absolute atmospheric correction

This class of methods attempts to deduce values for atmospheric parameters from information contained within the image itself rather than using externally-measured data. Each image is treated on its own.

$$\rho = \frac{\pi d^2(L - L_{haze})}{T_v(E_{sun} \cos \theta_z T_z + E_{down})} \quad (5)$$

The conversion of at-sensor radiance to atmospherically-corrected surface reflectance is described in Equation 5. Absolute atmospheric correction methods use measurements or atmospheric simulation models to determine the parameters  $T_z$ ,  $T_v$ ,  $E_{down}$ , and  $L_{haze}$  (Chavez 1989). The major difference between the relative atmospheric correction methods is the procedure for estimating these values. With default parameter choices, this simplifies to the equation for at-sensor reflectance (Table 4; Equation 4).

#### *Dark object subtraction*

The dark object subtraction (DOS) method assumes that if there are areas in an image with very low actual reflectance values, any apparent reflectance should be due to atmospheric scattering effects, and this information can be used to calibrate the rest of the image (Chavez 1988, 1989). The darkest pixels can be selected by examining the histogram of the  $DN$  values in an image, or by setting a threshold such as ‘lowest  $DN$  value found in at least  $n$  pixels,’ or some other criterion appropriate for the size of image being analyzed. The chosen  $DN$  value, the Starting Haze Value ( $SHV$ ) is then converted to radiance (e.g., Equation 2 or similar conversion). It is unlikely that most images contain entire pixels that are true black, so a correction is applied that assumes a 1% actual reflectance of these areas.

$$\begin{aligned} L_{1\%} &= 0.01 \frac{E_{sun} \cos \theta_z}{\pi d^2} \\ L_{haze} &= SHV_{rad} - L_{1\%} \end{aligned} \quad (6)$$

The simplest form of DOS simply converts the calculated  $L_{haze}$  value to at-sensor reflectances (Equation 4) and subtracts it from the entire image (also converted to at-sensor reflectances). A new  $SHV$  value must be calculated for each band (Chavez 1988).

The improved method developed by Chavez (1989) uses information from a single band to calculate  $L_{haze}$  values for the remaining bands of an image. This method produces correlated haze values, and may be more accurate if there are few shadows or dark areas. Scattering is band-specific, and the band effects are correlated with atmospheric conditions. The DOS method implemented here uses a realistic relative atmospheric scattering model, and maintains the spectral relationship between bands (Chavez 1989). This may be important for vegetation

Model	$T_z$	$T_v$	$E_{down}$	$L_{haze}$
Apparent reflectance	1	1	0	0
DOS	1	1	0	$SHV$
COSTZ	$\cos \theta_z$	$\cos \theta_v$	0	$SHV$
DOS4	Iterative	Iterative	Iterative	Iterative

Table 4: Parameters values used in four different atmospheric correction methods.

indices whose values depend on the ratios between bands. The DOS method works poorly for bands 5 and 7, hugely overestimating the  $L_{haze}$  value. Only small components of the total atmospheric scattering occurs in these bands, so the *DN* corrections for very clear atmosphere were used for bands 5 and 7. The `DOS()` function will take the *SHV* value for the starting band (usually Band 1, though bands 2 or 3 may be used), and calculate the related *SHV* value for each other band.

DOS correction as implemented here is a two-step process. In this example, the July image is corrected. Band 1 is used to find the *SHV*, here the lowest *DN* with at least 1000 pixels.

```
R> SHV <- table(july1@data[, 1])
R> SHV <- min(as.numeric(names(SHV)[SHV > 1000]))
R> SHV
```

```
[1] 69
```

That *SHV* (69) is then used in `DOS()` to find the corrected *SHV* values for the remaining bands (Chavez 1989).

```
R> july.DOS <- DOS(sat = 7, SHV = SHV, SHV.band = 1, Grescale = 0.77569,
+   Brescale = -6.2, sunelev = 61.4, edist = ESdist("2002-07-20"))
R> july.DOS <- july.DOS[["DNfinal.mean"]]
R> july.DOS
```

	coef-4	coef-2	coef-1	coef-0.7	coef-0.5
band1	68.308152	68.30815	68.30815	68.30815	68.30815
band2	41.927435	53.23414	60.23021	62.53285	64.12406
band3	25.580966	40.56327	52.31547	56.60737	59.69712
band4	14.858007	28.34164	43.02630	49.22788	53.96081
band5	8.443139	13.20415	25.72192	33.59098	40.69352
band7	8.130282	10.87164	21.16987	28.78982	36.18461

The above R output shows the possible *SHV* values calculated for five scattering coefficients, with the smallest coefficient (-4) describing the clearest conditions and -0.5 representing extreme haze. For this example, Band 1 was used to calculate the *SHV* from the actual image, so it is not adjusted for scattering coefficient. The user must select the appropriate set of band-specific *SHV* values. Chavez (1989) suggested using the original *SHV* as a guide:  $SHV \leq 55$  very clear (-4);  $SHV$  56–75 clear (-2);  $SHV$  76–95 moderate (-1);  $SHV$  96–115 hazy (-0.7);  $SHV > 115$  very hazy (-0.5). The *SHV* for Band 1 from July was 69, so the atmosphere was clear, and the corresponding column `coef-2` was selected for use in `DOS()`.

```
R> july.DOS <- july.DOS[, 2]
R> july2.DOSrefl <- radiocorr(july2, Grescale = 0.79569, Brescale = -6.4,
+   sunelev = 61.4, edist = ESdist("2002-07-20"), Esun = 1812,
+   Lhaze = july.DOS[2], method = "DOS")
R> july4.DOSrefl <- radiocorr(july4, Grescale = 0.63725, Brescale = -5.1,
+   sunelev = 61.4, edist = ESdist("2002-07-20"), Esun = 1039,
+   Lhaze = july.DOS[4], method = "DOS")
R> july4.DOSrefl@data[!is.na(july.cloud@data[, 1]), 1] <- NA
```

*COSTZ*

Chavez (1996) improved on his earlier dark object subtraction methods by adding a correction for the multiplicative transmittance component of the atmospheric scatter ( $\cos \theta_z$ , abbreviated as COSTZ). In this revised procedure,  $\cos \theta_z$  is used as an approximation of  $T_z$ , and  $\cos \theta_v$  is used as an approximation of  $T_v$ . For Landsat, the latter parameter is one because the satellite sensor has a nadir view ( $\theta_v = 0^\circ$ ). The value for  $L_{haze}$  is determined just as for the DOS method. This method is not appropriate for use with bands 5 or 7; the original DOS method should be used with these data (Song, Woodcock, Seto, Lenney, and Macomber 2001).

```
R> july4.COSTZrefl <- radiocorr(july4, Grescale = 0.63725, Brescale = -5.1,
+   sunelev = 61.4, edist = ESdist("2002-07-20"), Esun = 1039,
+   Lhaze = july.DOS[4], method = "COSTZ")
R> july4.COSTZrefl@data[!is.na(july.cloud@data[, 1]), 1] <- NA
```

*Modified dark object subtraction*

The modified dark object subtraction method (DOS4) was developed to incorporate the effect of atmospheric aerosols into atmospheric correction (Song *et al.* 2001). The value for  $L_{haze}$  calculated in the DOS method is used. Corrected values for  $T_z$  and  $T_v$  are determined through an iterative process. Both are set to initial values of one, and Equation 7 is solved for  $\tau$ , the Rayleigh atmospheric optical depth. New values are calculated for  $T_z$  and  $T_v$  (Equation 8), and the process is repeated until  $\tau$  stabilizes. This generally requires fewer than ten iterations.

$$\tau = -\cos \theta_z \ln \left( 1 - \frac{G_{rescale} DN_{min} + B_{rescale} - 0.01(E_o \cos \theta_z T_z + E_{down})T_v/\pi}{E_o \cos \theta_z} \right) \quad (7)$$

$$\begin{aligned} T_v &= \exp(-\tau / \cos \theta_v) \\ T_z &= \exp(-\tau / \cos \theta_z) \end{aligned} \quad (8)$$

```
R> july4.DOS4refl <- radiocorr(july4, Grescale = 0.63725, Brescale = -5.1,
+   sunelev = 61.4, edist = ESdist("2002-07-20"), Esun = 1039,
+   Lhaze = july.DOS[4], method = "DOS4")
R> july4.DOS4refl@data[!is.na(july.cloud@data[, 1]), 1] <- NA
```

When compared to at-sensor reflectance, all three absolute atmospheric correction methods produced similar results for the July test image (Figure 4). Each reduced the dynamic range, but only slightly, and the overall appearance was similar to the original, unlike the results of most of the relative correction methods.

Other research has found that COSTZ was effective in the visible-light bands (1-3), but less accurate in the near-infrared, particularly in humid conditions (Wu, Wang, and Bauer 2005). Song *et al.* (2001) found that DOS4 outperformed COSTZ or DOS.

## 8. Topographic correction

The interaction between sun angle, surface slope and satellite position produces variations in surface reflectance unrelated to true reflectance. The same land use type can return a different

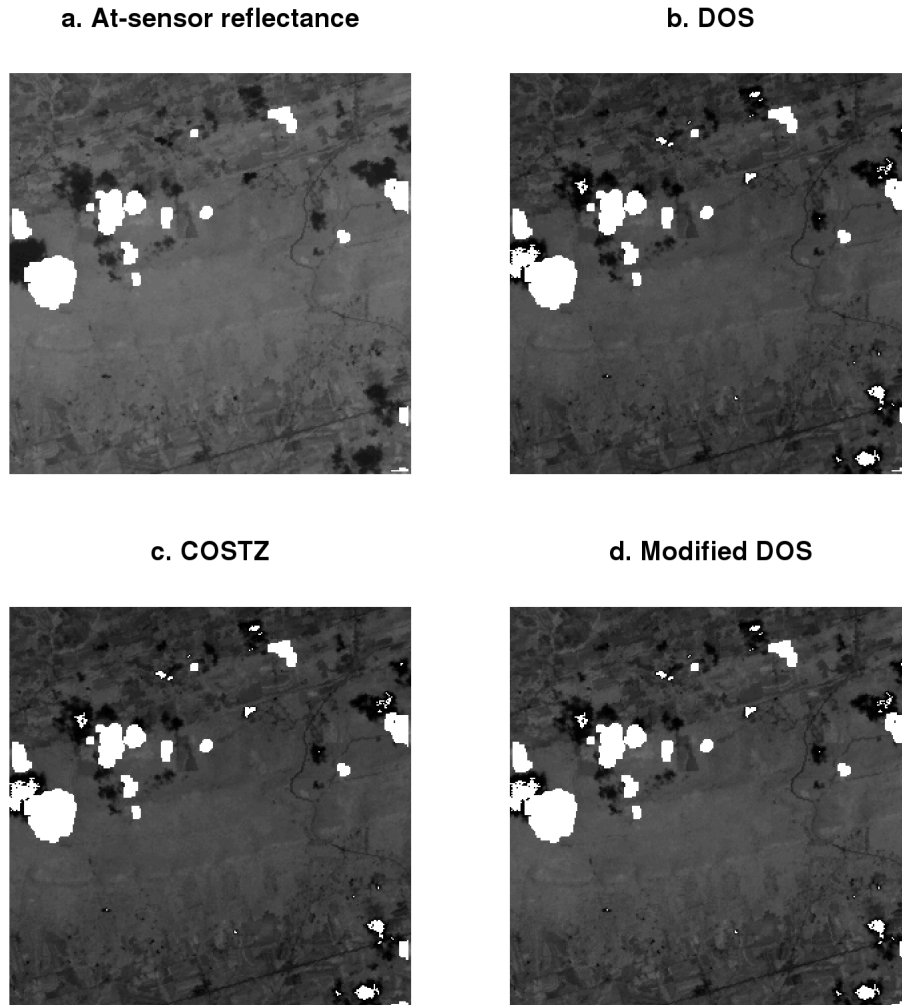


Figure 4: Absolute atmospheric corrections for Band 4 of the July data.

signal if located on opposite sides of a hill. The intent of topographic correction is to remove this source of variation, and leave only the portion of the reflectance signal actually due to ground cover, thus converting the reflectance from an inclined surface ( $\rho_T$ ) to that from an equivalent horizontal surface ( $\rho_H$ ).

The sun angle at the time of the November image was lower, so differential shading of the north and south faces of the ridge in the middle of the image can be clearly seen (Figure 1b, and see also Figure 1f). A successful topographic correction would eliminate this shading difference; corrected images should appear flat.

### 8.1. Illumination

Slope and aspect are used in conjunction with solar and satellite parameters to model illumination ( $IL$ ) conditions. Information derived from the DEM is required to compute the incident angle ( $\gamma_i$ ), defined as the angle between the normal to the ground and the sun rays.

The IL parameter varies from  $-1$  (minimum illumination) to  $1$  (maximum illumination) and is calculated from the slope angle  $\theta_p$ , solar zenith angle  $\theta_z$ , solar azimuth angle  $\phi_a$  and aspect angle  $\phi_o$  (Equation 9).

$$IL = \cos \gamma_i = \cos \theta_p \cos \theta_z + \sin \theta_p \sin \theta_z \cos (\phi_a - \phi_o) \quad (9)$$

The illumination is then used in one of several topographic correction methods. Seven such algorithms are currently implemented in `topocorr()`. Many of these algorithms are described and compared in [Riano \*et al.\* \(2003\)](#).

## 8.2. Lambertian methods

Lambertian methods assume that the reflectance for all wavelengths is constant regardless of viewing angle. The correction factor is identical across all bands.

### *Cosine correction*

The cosine method is a trigonometric approach that assumes that irradiance is proportional to the cosine of the incidence angle ([Teillet, Guindon, and Goodenough 1982](#)). The cosine correction discounts indirect illumination and saturates in dark areas.

$$\rho_H = \rho_T \left( \frac{\cos \theta_z}{IL} \right) \quad (10)$$

```
R> dem.slopeasp <- slopeasp(dem)
R> nov4.cosine <- topocorr(nov4.ar, dem.slopeasp$slope, dem.slopeasp$aspect,
+   sunelev = 26.2, sunazimuth = 159.5, method = "cosine")
```

### *Improved cosine correction*

The improved cosine method attempts to compensate for the overcorrection often seen in the cosine method by including average illumination ( $\overline{IL}$ ) in the calculation ([Civco 1989](#)).

$$\rho_H = \rho_T + \left( \rho_T \left( \frac{\overline{IL} - IL}{\overline{IL}} \right) \right) \quad (11)$$

```
R> nov4.cosimp <- topocorr(nov4.ar, dem.slopeasp$slope, dem.slopeasp$aspect,
+   sunelev = 26.2, sunazimuth = 159.5, method = "improvedcosine")
```

### *Gamma correction*

The Gamma method is an extension of the cosine correction that adds terms for the sensor view angle on flat terrain ( $\theta_v$ ) and on inclined terrain ( $\beta_v$ ). This is another attempt to reduce overcorrection in areas with low illumination ([Richter, Kellenberger, and Kaufmann 2009](#)).

$$\rho_H = \rho_T \gamma = \rho_T \left( \frac{\cos \theta_z + \cos \theta_v}{IL + \cos \beta_v} \right) \quad (12)$$

$$\beta_v = 90^\circ - (\theta_v + \theta_p)$$

```
R> nov4.gamma <- topocorr(nov4.ar, dem.slopeasp$slope, dem.slopeasp$aspect,
+   sunelev = 26.2, sunazimuth = 159.5, method = "gamma")
```

### *Sun-canopy-sensor method*

The sun-canopy-sensor method (SCS) was developed by [Gu and Gillespie \(1998\)](#) for use in forested areas where the canopy geometry contributes to reflectance on a sloped surface ([Gao and Zhang 2009](#)).

$$\rho_H = \rho_T \left( \frac{\cos \theta_z \cos \theta_p}{IL} \right) \quad (13)$$

```
R> nov4.SCS <- topocorr(nov4.ar, dem.slopeasp$slope, dem.slopeasp$aspect,
+   sunelev = 26.2, sunazimuth = 159.5, method = "SCS")
```

## 8.3. Non-Lambertian methods

This group of methods recognizes that the combination of angles of incidence and observation can affect reflectance: surface roughness matters.

### *Minnaert method*

The Minnaert method adds a band-specific constant  $K$  to the cosine method ([Minnaert 1941](#), in [Riano et al. 2003](#); Equation 14). If  $K = 1$ , the Minnaert and cosine methods are equivalent (Lambertian behavior is assumed).

$$\rho_H = \rho_T \left( \frac{\cos \theta_z}{IL} \right)^K \quad (14)$$

The  $K$  parameter is the slope of the ordinary linear regression with  $K$  and  $\ln \rho_H$  as regression coefficients, and is constant across the entire image for each band (Equation 15).

$$\ln(\rho_T) = \ln(\rho_H) + K \ln \frac{IL}{\cos \theta_z} \quad (15)$$

The `topocorr()` function with the argument `method = "minnaert"` will take care of both steps, returning the corrected image.

```
R> nov4.minnaert <- topocorr(nov4.ar, dem.slopeasp$slope, dem.slopeasp$aspect,
+   sunelev = 26.2, sunazimuth = 159.5, method = "minnaert")
```

A further modification of the Minnaert method includes the slope explicitly as well as through the illumination calculation ([Colby 1991](#); Equation 16).

$$\rho_H = \rho_T \cos \theta_p \left( \frac{\cos \theta_z}{IL \cos \theta_p} \right)^K \quad (16)$$

```
R> nov4.min2 <- topocorr(nov4.ar, dem.slopeasp$slope, dem.slopeasp$aspect,
+   sunelev = 26.2, sunazimuth = 159.5, method = "minslope")
```

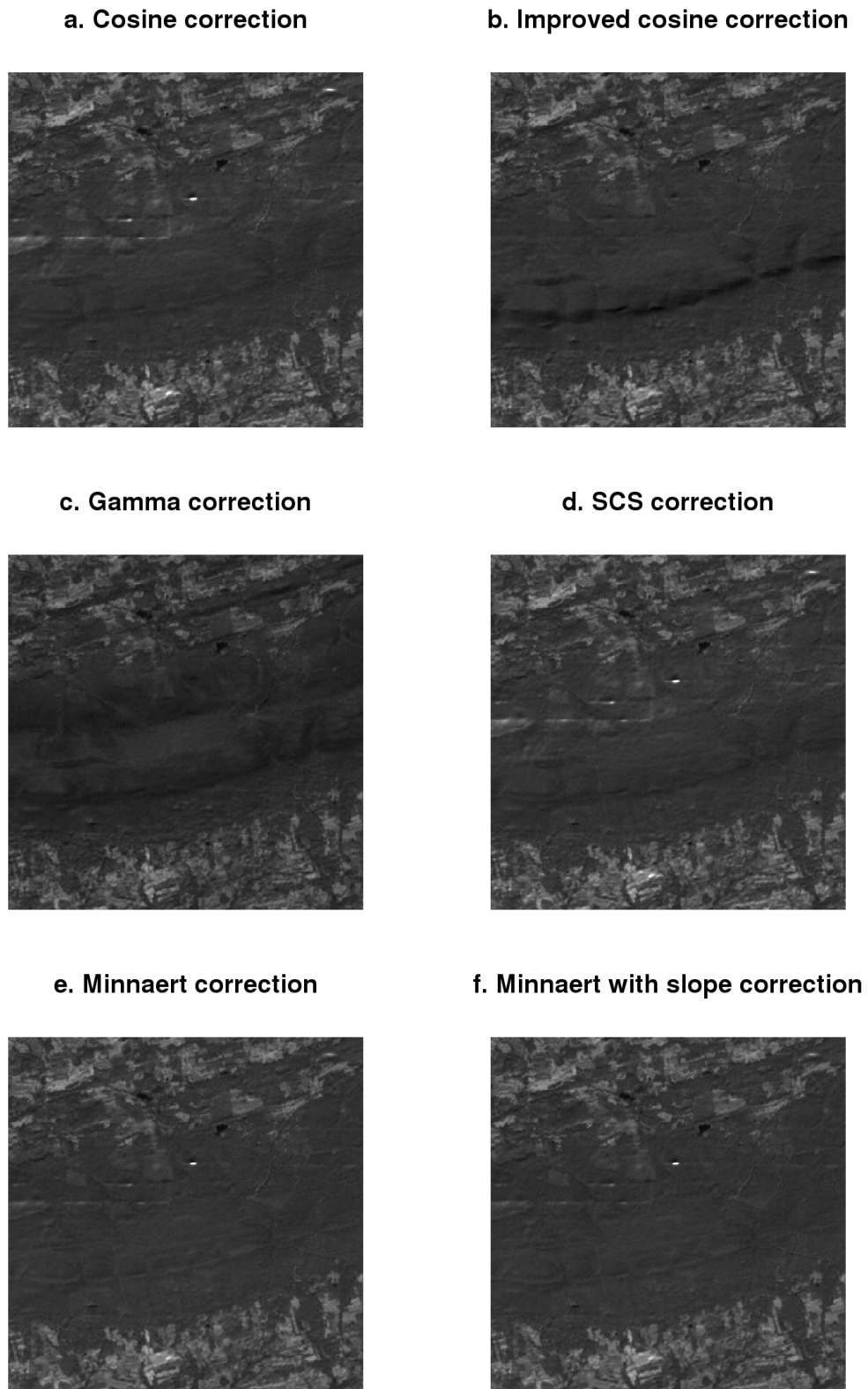


Figure 5: Topographic corrections for Band 4 of the November data.

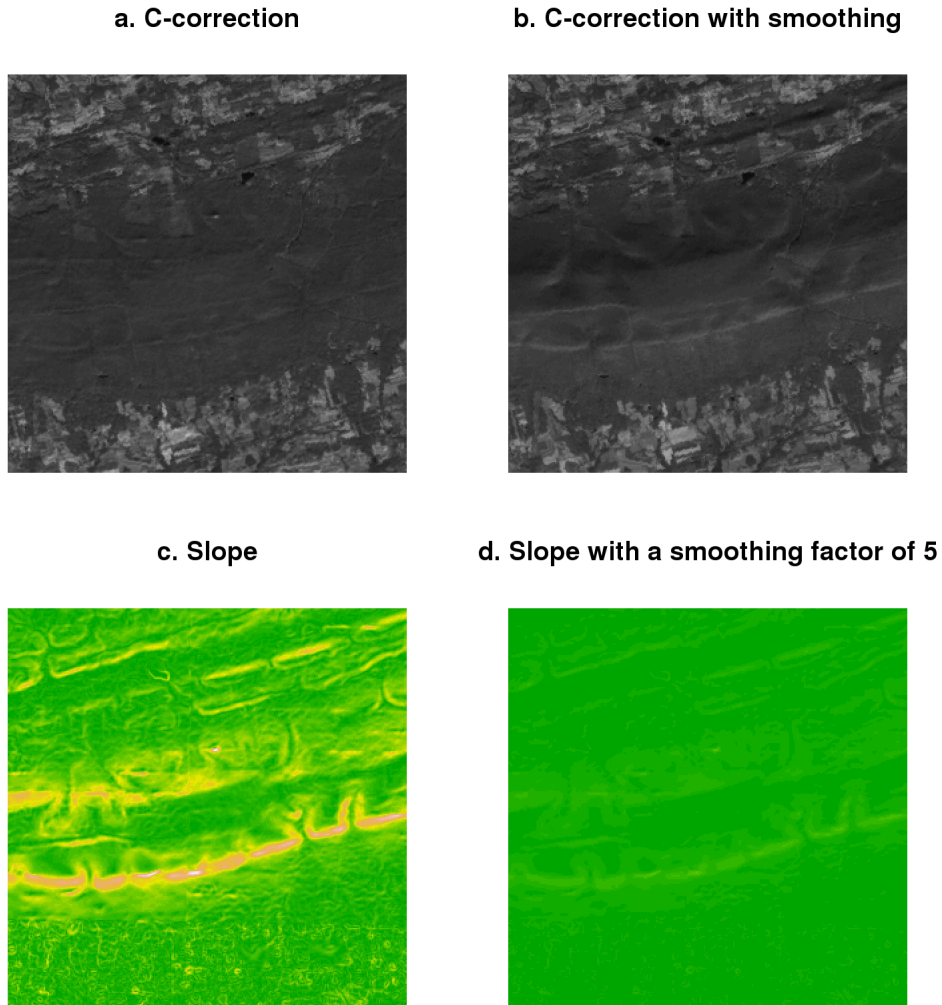


Figure 6: Topographic corrections for Band 4 of the November data (continued).

### *C-correction*

The C-correction method is a statistical approach based on the ratio of the band-specific regression coefficients  $b$  and  $m$ , as given in Equation 17 (Teillet *et al.* 1982).

$$\begin{aligned}\rho_H &= \rho_T \left( \frac{\cos \theta_z + c}{IL + c} \right) \\ \rho_T &= b + mIL \\ c &= \frac{b}{m}\end{aligned}\tag{17}$$

```
R> nov4.ccor <- topocorr(nov4.ar, dem.slopeasp$slope, dem.slopeasp$aspect,
+   sunelev = 26.2, sunazimuth = 159.5, method = "ccorrection")
```

Riano *et al.* (2003) recommend smoothing the slope to reduce the overcorrection imposed when the illumination is low. A smoothing option was added to `slopeasp()` to make this

variant possible. They found the most improvement with a slope correction factor of 5, as illustrated in the example.

```
R> dem.smooth5 <- slopeasp(dem, smoothing = 5)
R> nov4.ccorsmooth <- topocorr(nov4.ar, dem.smooth5$slope, dem.smooth5$aspect,
+   sunelev = 26.2, sunazimuth = 159.5, method = "ccorrection")
```

None of the topographic correction methods completely eliminated the shading effects due to the central ridge (Figures 5, 6). The gamma correction was particularly poor (Figure 5c), as was the C-correction (Figure 6a). The cosine and Minnaert methods performed the best, but in all the images the north-south topographic features along the main ridge can be clearly seen.

The cosine and SCS methods also resulted in reflectances greater than one. The Minnaert methods increased the dynamic range, though not the median, and the gamma correction reduced both. Meyer, Itten, Kellenberger, Sandmeier, and Sandmeier (1993) found that the Minnaert and C-correction methods gave similar results, but that the cosine method results were very different. Other work found that Minnaert was superior under most conditions (Richter *et al.* 2009).

## 9. Conclusions

Implementing atmospheric and topographic correction methods in R was straightforward, given R's good preexisting spatial capabilities. While large-scale production work is probably best done in a GIS environment, the scripting features available in R make it a feasible solution for small- and medium-sized tasks involving satellite remote sensing imagery.

The **landsat** package will be useful for researchers investigating the utility of these algorithms for their own work, and for facilitating development of new methods. The topographic algorithms especially appear to need further research. The wide range of sophisticated statistical tools available in R make it suitable for research and development on these methods. The open source nature of both R and of the **landsat** package allow for examination and alteration of the code base, facilitating further work on processing satellite imagery.

## Acknowledgments

This work contributes to the Conservation Effects Assessment Project (CEAP), jointly funded, coordinated and administered by the United States Department of Agriculture's Natural Resources Conservation Service, Agricultural Research Service, and Cooperative State Research, Education, and Extension Service. Funding for this project was provided by the USDA-NRCS. Forrest R. Stevens provided considerable assistance in locating a problem with an earlier version of **landsat**.

Mention of trade names or commercial products in this publication is solely for the purpose of providing specific information and does not imply recommendation or endorsement by the US Department of Agriculture.

USDA is an equal opportunity provider and employer.

## References

- Bivand RS, Pebesma EJ, Gomez-Rubio V (2008). *Applied Spatial Data Analysis with R*. Springer-Verlag, New York.
- Chander G, Markham BL, Helder DL (2009). “Summary of Current Radiometric Calibration Coefficients for Landsat MSS, TM, ETM+, and EO-1 ALI Sensors.” *Remote Sensing of Environment*, **113**, 893–903.
- Chavez Jr PS (1988). “An Improved Dark-Object Subtraction Technique for Atmospheric Scattering Correction of Multispectral Data.” *Remote Sensing of Environment*, **24**, 459–479.
- Chavez Jr PS (1989). “Radiometric Calibration of Landsat Thematic Mapper Multispectral Images.” *Photogrammetric Engineering and Remote Sensing*, **55**, 1285–1294.
- Chavez Jr PS (1996). “Image-Based Atmospheric Corrections Revisited and Improved.” *Photogrammetric Engineering and Remote Sensing*, **62**, 1025–1036.
- Civco DL (1989). “Topographic Normalization of Landsat Thematic Mapper Digital Imagery.” *Photogrammetric Engineering and Remote Sensing*, **55**, 1303–1309.
- Clarke KC, Lee SJ (2007). “Spatial Resolution and Algorithm Choice as Modifiers of Downslope Flow Computed from Digital Elevation Models.” *Cartography and Geographic Information Science*, **34**, 215–230.
- Colby JD (1991). “Topographic Normalization in Rugged Terrain.” *Photogrammetric Engineering and Remote Sensing*, **57**, 531–537.
- Crist EP (1985). “A TM Tasseled Cap Equivalent Transformation for Reflectance Factor Data.” *Remote Sensing of Environment*, **17**, 301–306.
- Crist EP, Kauth RJ (1986). “The Tasseled Cap De-Mystified.” *Photogrammetric Engineering and Remote Sensing*, **52**, 81–86.
- Gao Y, Zhang W (2009). “LULC Classification and Topographic Correction of Landsat-7 ETM+ Imagery in the Yangjia River Watershed: The Influence of DEM Resolution.” *Sensors*, **9**, 1980–1995.
- GDAL Development Team (2011). *GDAL – Geospatial Data Abstraction Library, Version 1.7.3*. Open Source Geospatial Foundation. URL <http://www.gdal.org/>.
- Gu D, Gillespie A (1998). “Topographic Normalization of Landsat TM Images of Forest Based on Subpixel Sun-Canopy-Sensor Geometry.” *Remote Sensing of Environment*, **64**, 166–175.
- Hall FG, Strebel DE, Nickeson JE, Goetz SJ (1991). “Radiometric Rectification: Toward a Common Radiometric Response Among Multidate, Multisensor Images.” *Remote Sensing of Environment*, **35**, 11–27.
- Huang C, Wylie B, Yang L, Homer C, Zylstra G (2002). “Derivation of a Tasseled Cap Transformation Based on Landsat 7 At-Satellite Reflectance.” *International Journal of Remote Sensing*, **23**, 1741–1748.

- Keitt TH, Bivand R, Pebesma E, Rowlingson B (2011). *rgdal: Bindings for the Geospatial Data Abstraction Library*. R package version 0.7-1, URL <http://CRAN.R-project.org/package=rgdal>.
- Legendre P (2008). *lmodel2: Model II Regression*. R package version 1.6-3, URL <http://CRAN.R-project.org/package=lmodel2>.
- Martinuzzi S, Gould WA, González OMR (2007). “Creating Cloud-Free Landsat ETM+ Data Sets in Tropical Landscapes: Cloud and Cloud-Shadow Removal.” *General Technical Report IITF-GTR-32*, United States Department of Agriculture Forest Service International Institute of Tropical Forestry.
- Meyer P, Itten KI, Kellenberger T, Sandmeier S, Sandmeier R (1993). “Radiometric Corrections of Topographically Induced Effects on Landsat TM Data in an Alpine Environment.” *ISPRS Journal of Photogrammetry and Remote Sensing*, **48**, 17–28.
- Minnaert M (1941). “The Reciprocity Principle in Lunar Photometry.” *Astrophysics Journal*, **37**, 978–986.
- R Development Core Team (2011). *R: A Language and Environment for Statistical Computing*. R Foundation for Statistical Computing, Vienna, Austria. ISBN 3-900051-07-0, URL <http://www.R-project.org/>.
- Riano D, Chuvieco E, Salas J, Aguado I (2003). “Assessment of Different Topographic Corrections in Landsat-TM Data for Mapping Vegetation Types.” *IEEE Transactions on Geoscience and Remote Sensing*, **41**, 1056–1061.
- Richter R, Kellenberger T, Kaufmann H (2009). “Comparison of Topographic Correction Methods.” *Remote Sensing*, **1**, 184–196.
- Schott JR, Salvaggio C, Volchok WJ (1988). “Radiometric Scene Normalization Using Pseudoinvariant Features.” *Remote Sensing of Environment*, **26**, 1–16.
- Song C, Woodcock CE, Seto KC, Lenney MP, Macomber SA (2001). “Classification and Change Detection Using Landsat TM Data: When and How to Correct Atmospheric Effects?” *Remote Sensing of Environment*, **75**, 230–244.
- Teillet PM, Guindon B, Goodenough DG (1982). “On the Slope-Aspect Correction of Multi-spectral Scanner Data.” *Canadian Journal of Remote Sensing*, **8**, 84–106.
- Unwin D (1981). *Introductory Spatial Analysis*. Methuen, London.
- US Geological Survey (2010a). “Earth Resources Observation and Science Center.” Accessed 2010-09-20, URL <http://eros.usgs.gov/>.
- US Geological Survey (2010b). “Landsat Missions.” Accessed 2010-09-20, URL <http://landsat.usgs.gov/>.
- Wu J, Wang D, Bauer ME (2005). “Image-Based Atmospheric Correction of QuickBird Imagery of Minnesota Cropland.” *Remote Sensing of Environment*, **99**, 315–325.

## A. Mathematical quantities

$DN$  – Digital number (integer, 0–255 for Landsat).

$\lambda$  – Wavelength ( $\mu m$ ).

$L$  – At-sensor radiance ( $Wm^{-2}sr^{-1}\mu m^{-1}$ ).

$\rho_{AS}$  – At-sensor reflectance (unitless).

$\rho$  – Surface reflectance (unitless).

$G_{rescale}$  – Band-specific gain ( $Wm^{-2}sr^{-1}\mu m^{-1}DN^{-1}$ ).

$B_{rescale}$  – Band-specific bias ( $Wm^{-2}sr^{-1}\mu m^{-1}$ ).

$gain_2$  – Band-specific gain (alternate version).

$offset$  – Band-specific (alternate version).

$L_{max}$  – Radiance associated with maximum  $DN$  value ( $Wm^{-2}sr^{-1}\mu m^{-1}$ ).

$L_{min}$  – Radiance associated with minimum  $DN$  value ( $Wm^{-2}sr^{-1}\mu m^{-1}$ ).

$DN_{max}$  – Maximum  $DN$  value, usually 255.

$DN_{min}$  – Minimum  $DN$  value, usually 0.

$E_{sun}$  – Band-specific exoatmospheric solar constant ( $Wm^{-2}\mu m^{-1}$ ).

$d$  – Earth-Sun distance (AU).

$E_o$  – Distance-adjusted exoatmospheric solar constant  $d^2/E_{sun}$ .

$\theta_z$  – Solar zenith angle (degrees);  $90^\circ - \theta_s$ .

$\theta_s$  – Solar elevation angle (degrees).

$DOY$  – Day of year; Julian date (days).

$L_{haze}$  – Path radiance, upwelling atmospheric scattering ( $Wm^{-2}sr^{-1}\mu m^{-1}$ ).

$T_v$  – Atmospheric transmittance from surface to the sensor ( $Wm^{-2}\mu m^{-1}$ ).

$T_z$  – Atmospheric transmittance from the Sun to the surface ( $Wm^{-2}\mu m^{-1}$ ).

$E_{down}$  – Downwelling irradiance due to atmospheric scattering ( $Wm^{-2}\mu m^{-1}$ ).

$SHV$  – Starting haze value ( $DN$ ).

$Z$  – Elevation at pixel  $(i, j)$ .

$EW$  – East-west component of slope.

$NS$  – North-south component of slope.

$EW_{res}$  – East-west pixel resolution.

$NS_{res}$  – North-south pixel resolution.

$\theta_p$  – Slope angle (degrees).

$\theta_z$  – Solar zenith angle (degrees).

$\theta_v$  – Sensor zenith angle (degrees;  $0^\circ$  for Landsat).

$\beta_v$  – Sensor view angle on inclined terrain (degrees).

$\phi_a$  – Solar azimuth angle (degrees)

$\phi_o$  – Aspect angle (degrees, with north =  $0^\circ$  and moving clockwise).

$\rho_H$  – Reflectance of a horizontal surface (unitless).

$\rho_T$  – Reflectance of an inclined surface (unitless).

$IL$  – Illumination ( $-1$  to  $+1$ ).

$\overline{IL}$  – Average illumination across the image ( $-1$  to  $+1$ ).

$\gamma_i$  – Incident angle between the normal to the ground and the sun rays (degrees).

$\tau$  – Rayleigh atmospheric optical depth.

**Affiliation:**

Sarah C. Goslee

USDA-ARS Pasture Systems and Watershed Management Research Unit

Bldg. 3702 Curtin Rd.

University Park PA, 16802, United States of America

E-mail: [Sarah.Goslee@ars.usda.gov](mailto:Sarah.Goslee@ars.usda.gov)